

Mechanical Detection of Nuclear Decays

Jiaxiang Wang¹, T. W. Penny¹, Juan Recoaro¹, Benjamin Siegel¹, Yu-Han Tseng¹, and David C. Moore^{1,2}

¹Wright Laboratory, Department of Physics, Yale University, New Haven, Connecticut 06520, USA

²Yale Quantum Institute, Yale University, New Haven, Connecticut 06520, USA



(Received 30 January 2024; accepted 23 April 2024; published 8 July 2024)

We report the detection of individual nuclear α decays through the mechanical recoil of the entire micron-sized particle in which the decaying nuclei are embedded. Momentum conservation ensures that such measurements are sensitive to any particles emitted in the decay, including neutral particles that may otherwise evade detection with existing techniques. Detection of the minuscule recoil of an object more than 10^{12} times more massive than the emitted particles is made possible by recently developed techniques in levitated optomechanics, which enable high-precision optical control and measurement of the mechanical motion of optically trapped particles. Observation of a change in the net charge of the particle coincident with the recoil allows decays to be identified with background levels at the micro-Becquerel level. The techniques developed here may find use in fields ranging from nuclear forensics to dark matter and neutrino physics.

DOI: [10.1103/PhysRevLett.133.023602](https://doi.org/10.1103/PhysRevLett.133.023602)

Introduction.—Accurate detection of nuclear decays is central to a variety of fields in physics, engineering, and medicine. The vast majority of detectors for such decays rely on measuring the energy deposited by decay products, typically through generation of ionization, scintillation, or phonons (heat) in a detection medium [1]. However, these technologies ultimately rely on the decay products themselves to interact in the detector and deposit most of their energy, allowing particles that exit the detector to evade detection. A well-known example is nuclear β decay, where the emitted neutrino will escape any practical detector, and only a fraction of the total decay energy is detected with conventional techniques.

An alternative approach is to reconstruct the momentum imparted to the object containing the decaying nucleus by the recoil of its daughter, following the escape of the primary decay products [2]. This momentum-based reconstruction is sensitive to any escaping particles, including neutral particles, and has been demonstrated for individual recoiling nuclei [3,4]. However, the tiny recoil has been previously undetectable for a much more massive solid object containing the decaying nucleus. For example, the α decays detected here impart a momentum impulse of only $\sim 10^{-19}$ kg m/s to the micron-sized spheres containing the decaying nuclei.

Detection of such tiny recoils requires extreme isolation of the object containing the decaying nucleus from thermal noise and precise measurement of the object's motion. These stringent requirements can now be met by rapid progress in the optomechanical control and measurement of levitated particles [5]. By optically trapping nano to micron-size particles in high vacuum, thermal noise can be made negligible [6]. The interaction of the trapped

particle with the laser used to detect its position then provides the dominant noise source [5–7]. Ultimately, the minimal possible measurement induced noise is constrained by quantum mechanics [8,9], and particles as large as a femtogram in mass (100 nm in diameter) are now reaching the quantum measurement regime [10–15]. Such particles are extremely precise force sensors [16,17], finding applications in tests of quantum mechanics with massive objects [18–22], searches for new short-distance interactions [23,24], dark matter [25–28], gravitational waves [29,30], and neutrino physics [31].

Here, we demonstrate the detection of individual nuclear α decays using optically levitated micron-sized spheres (with mass > 10 pg). Decays are detected through the change in the net electric charge of the particle following the decay and the coincident recoil of the entire particle. The combination of these signatures allows both extremely low backgrounds and sensitivity to the momentum carried by the decay products through the measurement of the recoil. While these techniques already reach signal-to-noise ratios above 10 for the recoil measurement, more than 100 times further improvement in the momentum sensitivity is expected as these larger spheres are also brought into the quantum measurement regime.

Experimental description.—In our experiment, we detect single nuclear decays occurring in silica spheres of radius ≈ 1.5 μm that are optically trapped in vacuum at pressures between 10^{-8} to 10^{-7} mbar. Before trapping, the spheres are implanted with ^{212}Pb , an unstable radon daughter in the thorium decay chain [Fig. 1(a)]. ^{220}Rn is introduced into an implantation chamber [32] where it undergoes α decay to produce $^{216}\text{Po}^+$ ions, which are drifted by an electric field to the sphere surfaces [Fig. 1(b)]. The ^{216}Po α decays then

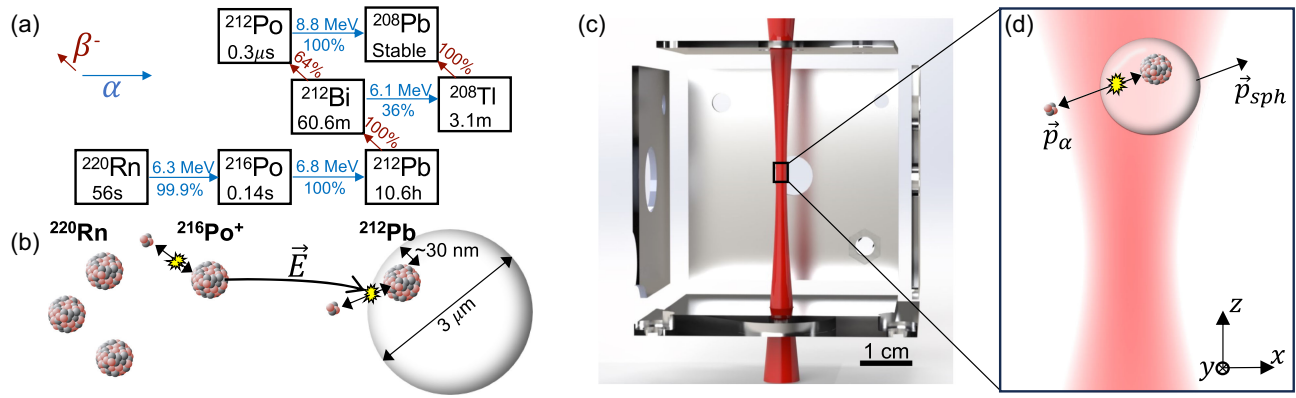


FIG. 1. (a) ^{220}Rn decay chain [40]. For each isotope, the decay half-life is given within the box. Arrows indicate the primary α decay energies and branching ratios (blue), as well as the relevant β decay branching ratios (red). (b) Schematic of ^{212}Pb implantation procedure described in the text. (c) Cross-sectional view of the electrodes surrounding the trap (an additional electrode on the front face and two weak imaging beams are not pictured). (d) Schematic of a sphere recoil following an α decay of ^{212}Bi or ^{212}Po , for which the daughter nucleus is stopped within the sphere while the α (and additional low-energy e^- and possibly secondary nuclear recoils, not pictured) exit the sphere. In this case, the momentum of the α particle can be inferred from the sphere recoil ($\vec{p}_\alpha = -\vec{p}_{\text{sph}}$).

implant ^{212}Pb daughters into the spheres at depths of $\lesssim 60$ nm. The implanted spheres are then transferred to a high-vacuum chamber and loaded into an optical trap formed by a focused laser, where the subsequent decays are measured.

The optical trap is surrounded by six planar electrodes [Fig. 1(c)]. The lower electrode is grounded, while the upper five can be biased independently. The electrodes and trapping beam define a coordinate system with the trapping beam propagating vertically in the z direction, and the x and y directions defined to be perpendicular to the electrode faces [Fig. 1(d)]. Once trapped in high vacuum, the sphere's net electric charge is determined by monitoring the sphere's motion in response to an oscillating electric field applied using these electrodes [7]. The net charge is calibrated into units of a single elementary charge, e , by observing discrete steps in the response [7,41,42], with the phase of the motion relative to the electric field determining the polarity. Electrons can be added to the sphere via thermionic emission from a tungsten filament or removed from the sphere via an ultraviolet lamp. The trapping beam is circularly polarized to rotate the sphere to $\gtrsim 100$ kHz rotational frequencies, gyroscopically stabilizing its motion and eliminating noise from fluctuations in its angular orientation [7,43]. The electrodes contain holes for the trapping beam and two weakly focused perpendicular imaging beams. The sphere position is detected by imaging the transmitted light on three detectors (one for each of x , y , and z). The dominant noise source in the x direction at the base pressure of 2×10^{-8} mbar is thermal noise from residual gas. The y and z directions suffer from additional technical noise due to fluctuations in the trapping beam pointing and intensity [7].

Charge measurement.—The results presented here consist of data from six spheres implanted with ^{212}Pb following

the procedure above. Each sphere is continuously measured for 2–3 days after loading into the optical trap and pumping to high vacuum. Once in vacuum, the charge is continuously monitored and individual decays occurring within the sphere are identified by detecting a change in the net charge of the sphere, ΔQ . Figure 2 a shows an example of the net charge of the sphere over time after reaching $< 10^{-7}$ mbar.

An automatic discharging procedure is implemented to maintain the net charge $|Q| < 50 e$. Discharging periods are recorded by the data acquisition system and excluded from the charge analysis [red lines in Fig. 2(a)]. Dead time due to the data acquisition, impulse response calibrations, and these discharging periods is $< 10\%$ of the total measurement time for all spheres considered.

For a typical implanted sphere, the decay frequency observed from these charge changes is initially around 2–5 decays per hour, with a decrease consistent with the ^{212}Pb half-life, $T_{1/2} = 10.6$ h [see Fig. 2(b)]. The background rate of charge changes was measured for an unimplanted sphere, with no charge changes observed in three days. As a result, any charge changes can be used to identify decays with backgrounds at the $< 1/(\text{day}) \sim \mu\text{Bq}$ level. For the measurements presented here, this charge measurement is crucial to reject transient noise bursts [32], which were found in previous work to be associated with vibrational or acoustic noise [27].

The distribution of charge changes from data across all spheres is shown in Fig. 2(c). While a detailed study of this distribution is beyond the scope of this work, several qualitative features are apparent. First, almost all charge changes are measured to be in the positive direction—i.e., the spheres nearly always lose more electrons than protons for both the α and β decays in the decay chain. Second, two peaks in the charge distribution are observed, and the data are empirically consistent with a Gaussian-like component

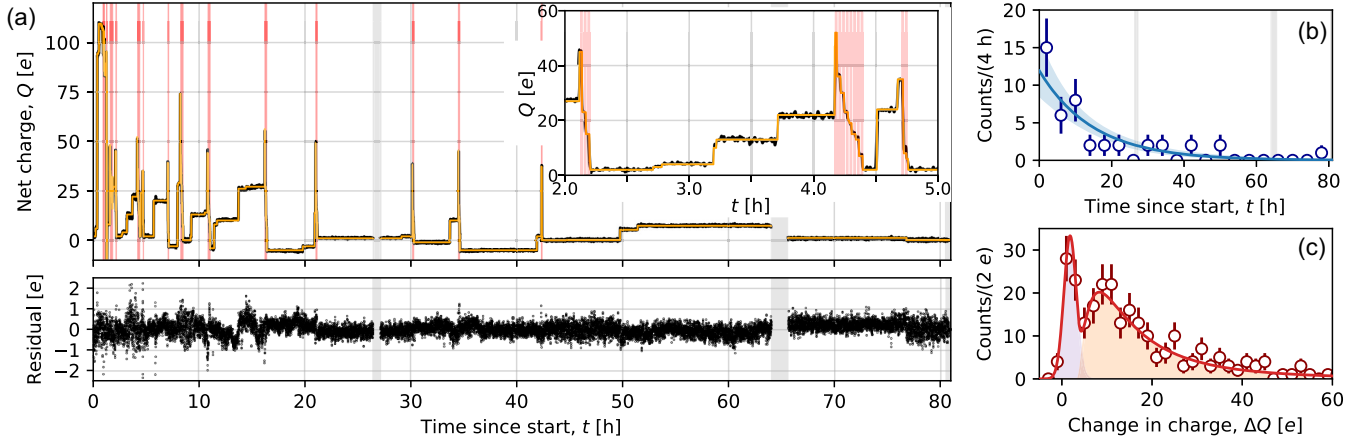


FIG. 2. (a) Upper panel: example of the measured charge versus time for a sphere implanted with ^{212}Pb . Positive values of the charge correspond to a net excess of protons over electrons in the sphere. The black line shows the measured sphere charge (averaged in 12 s intervals) while the orange line shows the best fit to these data after reconstructing the location of each charge change. Light red vertical lines show when the filament adding e^- to the sphere was active, while vertical gray bands indicate dead time during calibrations. The inset shows an enlargement of several charge changes near the beginning of the data. Lower panel: residual during the best-fit charge and the measured data. The residuals are typically $< 1 e$, demonstrating sensitivity to changes in the net charge of the sphere by a single e . (b) Example fit to the reconstructed number of charge changes versus time for the data shown on the left (blue points, with statistical error bars), with best fit $T_{1/2} = 10.3^{+1.8}_{-1.5}$ h (blue band). (c) Distribution of reconstructed charge changes for all spheres studied in this work, which is empirically consistent with a sum (red line) of the two components (shaded) described in the text.

peaking around $\Delta Q = +2 e$ and a heavy-tailed component (here modeled by a log-normal distribution) peaking around $\Delta Q = +8 e$, but with a tail of events extending to $\Delta Q \gg +50 e$. Of the 257 total observed decays, nine were observed with charge changes $> 60 e$ (beyond the range plotted in Fig. 2(c), with the largest observed change of $\Delta Q = +148 e$).

Recoil measurement.—The observed charge changes are used to tag decay events and provide timing information to search for recoils from the momentum transferred to the sphere during a decay. Since the time for all decay products to exit or stop within the sphere is much faster than its ~ 10 ms mechanical response time, the decay will impart an essentially instantaneous momentum impulse, which can be detected through the subsequent motion of the sphere’s center of mass.

To reconstruct the response of the sphere to such impulses, *in situ* calibrations are performed using electric impulses of known amplitude. Using the known net charge of the sphere and finite element method simulations of the electrode geometry, this calibration allows the impulse response to be measured to a relative accuracy of $< 2\%$ in the x and y directions, and to $< 10\%$ accuracy in the z direction, limited by uncertainty in the knowledge of the sphere position relative to the electrodes [32].

An “optimal filter” [32,44], making use of the calibrated impulse response and measured noise spectrum for each sphere, was found to provide the best resolution for impulse amplitude reconstruction. In the x direction, a resolution in the range of $\sigma_x = 15\text{--}27$ MeV/c was measured for the spheres considered. This corresponds to an expected

signal-to-noise ratio between 9 and 17 for a ^{212}Po α decay with energy $E_\alpha = 8.8$ MeV imparting its momentum $\sqrt{2m_\alpha E_\alpha} = 256$ MeV/c along the x direction, where m_α is the α particle mass. The resolution measured in the y and z directions is found to be poorer than in the x direction in our current system due to the larger impact of technical noise.

Figure 3 shows a candidate α decay coincident with an observed change in the charge of the sphere. The impulse amplitude reconstructed from the optimal filter, and calibrated using the *in situ* calibration described above, shows a recoil of the sphere coincident in time with the charge change (whose time can be reconstructed with < 100 ms precision), consistent with the impulse that would be expected for an α decay aligned between the x and y directions.

The distribution of reconstructed impulse amplitudes in the x direction coincident with detected charge changes for all spheres considered here is shown in Fig. 4. Compared to the charge data summarized in Fig. 2(c), this distribution contains fewer events (83 out of 257 total events) since only data periods at sufficiently low pressure that the sphere had reached a rotational velocity > 100 kHz and the noise was stable were considered for the recoil analysis, while all time periods were used in the charge analysis. Two of the six spheres were also not considered in this recoil analysis since they lacked *in situ* impulse calibrations. Only the x projection of the momentum is considered in the recoil analysis due to its higher signal-to-noise (and observed systematic drifts in the y amplitude between calibrations).

In Fig. 4, all reconstructed recoils are shown by the gray line, while only recoils coincident with charge changes for

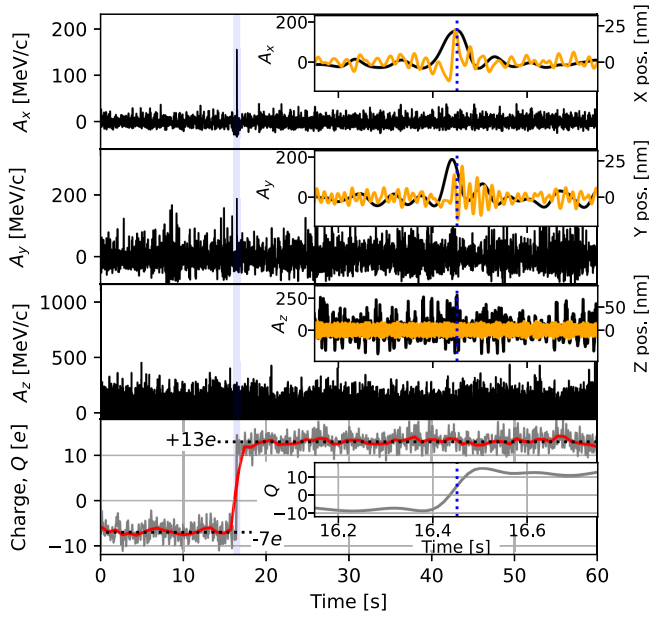


FIG. 3. Example reconstructed sphere recoil coincident with a charge change. The upper three panels show the filtered magnitude of the reconstructed impulse amplitude, A_j , for $j = x, y, z$ versus time. The insets show an enlargement of the region within ± 0.3 s of the reconstructed charge change time (light blue region in outer panel). A recoil is reconstructed in the x and y directions with a combined signal-to-noise ratio of 13 at the time indicated by the blue dotted line. The orange curve shows the reconstructed position (right axis) versus time, filtered around the resonant frequency for each direction, showing the expected damped harmonic oscillator response for x and y (and z response consistent with noise). The lower panel shows the reconstructed charge averaged over 25 ms (gray) and 1.6 s (red) windows.

which $\Delta Q < 30e$ are indicated by the blue points. The reconstructed amplitudes are corrected for the small impulse induced by the charge monitoring field in the x direction, which is estimated to provide negligible error after correction. The data with $\Delta Q < 30e$ are consistent with the expected distribution of momenta projected in the x direction based on a Monte Carlo simulation of the α decays from ^{212}Bi and ^{212}Po [32]. In addition to these α decays, the decay chain contains several β and γ transitions, which may occur in coincidence with the α decay. While these particles can carry non-negligible energy compared to the α , their relative momentum is much lower ($\sim 1\text{--}3$ MeV/c), and is not detectable with the resolution of the existing setup. The maximum momentum transfer occurs when the α particle escapes along the x direction and the daughter nucleus stops within the sphere.

A small fraction of the observed decays extend beyond the maximum momentum expected from these simulations. The cut removing events with $\Delta Q < 30e$ in Fig. 4 indicates that only events in the tail of the charge change distribution contribute to these unexpectedly large decays. Systematic checks were performed to ensure these large

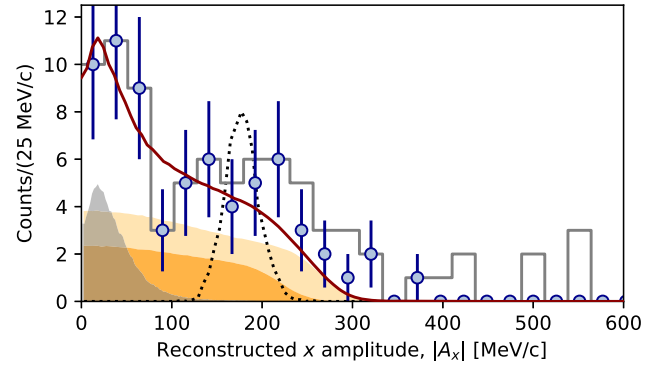


FIG. 4. Spectrum of the reconstructed x impulse amplitudes for each observed charge change. All data are shown by the gray histogram, while events with $\Delta Q < 30e$ are shown as blue points with error bars. The best fit to the spectrum (dark red line) is a sum of the predicted response from ^{212}Bi α decays (dark orange shaded), ^{212}Po α decays (light orange shaded), and β decays that impart momentum consistent with random sampling of the noise (gray shaded). The black dotted line shows the expected resolution for impulses in the x direction measured from the *in situ* calibrations.

reconstructed recoils were not due to miscalibration or reconstruction errors. While further study is required to definitively identify the origin of these recoils, these events may arise from decays in which the nuclear recoil is emitted along the sphere’s surface, leading to a large number of secondary nuclear recoils ejecting Si and O atoms. These ejected atoms may carry some fraction of their momentum in the direction of the emitted α , and might also produce the observed large changes in the net charge of the sphere as secondary electrons escape.

Discussion and outlook.—This work demonstrates the detection of single nuclear decays in optically trapped, micron-sized spheres through both the change in the sphere’s charge and its coincident recoil. While this initial work focuses on α decays, these techniques become especially powerful for decays in which weakly interacting neutral particles would escape conventional detectors. Extending the same techniques to femtogram mass spheres will allow reconstruction of the momentum of a single neutrino leaving the sphere with signal-to-noise > 100 [31]. Such techniques are generically sensitive to any “invisible” massive particles emitted in nuclear decays, including sterile neutrinos [31] or particles that may be related to dark matter [45,46].

Beyond fundamental physics, these techniques may find applications in nuclear forensics, which aims to determine the isotopic composition of a nuclear material [2,47]. While future work is required to fully characterize what background levels may be possible, from the measurements presented here it appears plausible that sub- μBq background rates will be achievable, possibly permitting detection of long-lived species such as ^{235}U in single captured

dust particles [2]. The measurements presented here will also allow the characterization of ejected radon daughters, as well as low-energy secondary electrons and ions, from decays near a solid surface, which may be relevant for applications in nuclear medicine [48,49] and rare event searches (e.g., [50–52]). Finally, the radon daughter decays ejecting > 100 low-energy e^- from a surface observed here may ultimately be observable in ion-based quantum computers, where a large number of charged particles passing through an ion array could simultaneously interact with multiple qubits [53]. Similar to phonon-mediated particle interactions in superconducting qubit arrays [54], these events may become evident only as error correction techniques begin to suppress uncorrelated errors and these systems are scaled to large size.

While this initial work has already demonstrated detection of single nuclear decays with signal-to-noise > 10 , substantial further improvement is expected. Future work is required to ensure the signal-to-noise is independent of the decay direction, characterize the background rates achievable, integrate conventional particle detectors around the trap, and to reach—and eventually surpass [55,56]—the “standard quantum limit” for the detection of the sphere recoil [9,57], where the momentum resolution would be $\sqrt{\hbar m \omega_0} \approx 50$ keV/c for the spheres considered here (with mass $m \sim 10$ pg and angular resonant frequency $\omega_0 \sim 2\pi \times 100$ Hz). The ongoing rapid progress in the field of levitated optomechanics promises to extend the future sensitivity of these techniques by orders of magnitude.

We thank Daniel Carney and Giorgio Gratta for useful discussions, and Fernando Monteiro and Gadi Afek for early work on the techniques used here. This work was supported through the DOE Office of Nuclear Physics, Quantum Horizons Award No. DE-SC0023672, and in part by ONR Grant No. N00014-23-1-2600 and NSF Grant No. PHY-2109329.

-
- [1] G. Knoll, *Radiation Detection and Measurement* (Wiley, New York, 2010).
- [2] A. Malyzhenkov, V. Lebedev, and A. Castro, *Phys. Rev. A* **98**, 052103 (2018).
- [3] M. M. Hindi, R. Avci, A. H. Hussein, R. L. Kozub, P. Miočinić, and L. Zhu, *Phys. Rev. C* **58**, 2512 (1998).
- [4] M. Trinczek *et al.*, *Phys. Rev. Lett.* **90**, 012501 (2003).
- [5] C. Gonzalez-Ballester, M. Aspelmeyer, L. Novotny, R. Quidant, and O. Romero-Isart, *Science* **374**, eabg3027 (2021).
- [6] J. Millen, T. S. Monteiro, R. Pettit, and A. N. Vamivakas, *Rep. Prog. Phys.* **83**, 026401 (2020).
- [7] F. Monteiro, W. Li, G. Afek, C.-I. Li, M. Mossman, and D. C. Moore, *Phys. Rev. A* **101**, 053835 (2020).
- [8] A. A. Clerk, M. H. Devoret, S. M. Girvin, F. Marquardt, and R. J. Schoelkopf, *Rev. Mod. Phys.* **82**, 1155 (2010).

- [9] J. Beckey, D. Carney, and G. Marocco, [arXiv:2311.07270](https://arxiv.org/abs/2311.07270).
- [10] U. Delić, M. Reisenbauer, K. Dare, D. Grass, V. Vuletić, N. Kiesel, and M. Aspelmeyer, *Science* **367**, 892 (2020).
- [11] L. Magrini, P. Rosenzweig, C. Bach, A. Deutschmann-Olek, S. G. Hofer, S. Hong, N. Kiesel, A. Kugi, and M. Aspelmeyer, *Nature (London)* **595**, 373 (2021).
- [12] F. Tebbenjohanns, M. L. Mattana, M. Rossi, M. Frimmer, and L. Novotny, *Nature (London)* **595**, 378 (2021).
- [13] A. Ranfagni, K. Børkje, F. Marino, and F. Marin, *Phys. Rev. Res.* **4**, 033051 (2022).
- [14] M. Kamba, R. Shimizu, and K. Aikawa, *Opt. Express* **30**, 26716 (2022).
- [15] J. Piotrowski, D. Windey, J. Vijayan, C. Gonzalez-Ballester, A. d. I. R. Sommer, N. Meyer, R. Quidant, O. Romero-Isart, R. Reimann, and L. Novotny, *Nat. Phys.* **19**, 1009 (2023).
- [16] T. Liang, S. Zhu, P. He, Z. Chen, Y. Wang, C. Li, Z. Fu, X. Gao, X. Chen, N. Li *et al.*, *Fundam. Res.* **3**, 57 (2023).
- [17] D. C. Moore and A. A. Geraci, *Quantum Sci. Technol.* **6**, 014008 (2021).
- [18] O. Romero-Isart, A. C. Pflanzer, F. Blaser, R. Kaltenbaek, N. Kiesel, M. Aspelmeyer, and J. I. Cirac, *Phys. Rev. Lett.* **107**, 020405 (2011).
- [19] M. Roda-Llodes, A. Riera-Campenya, D. Candoli, P. T. Grochowski, and O. Romero-Isart, *Phys. Rev. Lett.* **132**, 023601 (2024).
- [20] T. Weiss, M. Roda-Llodes, E. Torrontegui, M. Aspelmeyer, and O. Romero-Isart, *Phys. Rev. Lett.* **127**, 023601 (2021).
- [21] L. Neumeier, M. A. Ciampini, O. Romero-Isart, M. Aspelmeyer, and N. Kiesel, *Proc. Natl. Acad. Sci. U.S.A.* **121**, e2306953121 (2024).
- [22] B. A. Stickler, B. Papendell, S. Kuhn, B. Schirnski, J. Millen, M. Arndt, and K. Hornberger, *New J. Phys.* **20**, 122001 (2018).
- [23] C. P. Blakemore, A. Fieguth, A. Kawasaki, N. Priel, D. Martin, A. D. Rider, Q. Wang, and G. Gratta, *Phys. Rev. D* **104**, L061101 (2021).
- [24] A. A. Geraci, S. B. Papp, and J. Kitching, *Phys. Rev. Lett.* **105**, 101101 (2010).
- [25] C. J. Riedel, *Phys. Rev. D* **88**, 116005 (2013).
- [26] D. Carney *et al.*, *Quantum Sci. Technol.* **6**, 024002 (2021).
- [27] F. Monteiro, G. Afek, D. Carney, G. Krnjaic, J. Wang, and D. C. Moore, *Phys. Rev. Lett.* **125**, 181102 (2020).
- [28] G. Afek, D. Carney, and D. C. Moore, *Phys. Rev. Lett.* **128**, 101301 (2022).
- [29] N. Aggarwal, G. P. Winstone, M. Teo, M. Baryakhtar, S. L. Larson, V. Kalogera, and A. A. Geraci, [arXiv:2010.13157](https://arxiv.org/abs/2010.13157).
- [30] G. Winstone, Z. Wang, S. Klomp, R. G. Felsted, A. Laeuger, C. Gupta, D. Grass, N. Aggarwal, J. Sprague, P. J. Pauzuskie, S. L. Larson, V. Kalogera, and A. A. Geraci (LSD Collaboration), *Phys. Rev. Lett.* **129**, 053604 (2022).
- [31] D. Carney, K. G. Leach, and D. C. Moore, *PRX Quantum* **4**, 010315 (2023).
- [32] See Supplemental Material at <http://link.aps.org/supplemental/10.1103/PhysRevLett.133.023602>, which includes Refs. [33–39], for additional information about experimental methods and data analysis.
- [33] J. Ziegler, J. Biersack, and M. Ziegler, *SRIM, the Stopping and Range of Ions in Matter* (SRIM Company, Chester, Maryland, 2008).

- [34] SRIM 2013, <http://www.srim.org/>.
- [35] P. Hopke, *J. Radioanal. Nucl. Chem.* **203**, 353 (1996).
- [36] P. Pagelkopf and J. Porstendörfer, *Atmos. Environ.* **37**, 1057 (2003).
- [37] COMSOL Multiphysics v5.6, www.comsol.com. COMSOL AB, Stockholm, Sweden.
- [38] C. P. Blakemore, A. D. Rider, S. Roy, A. Fieguth, A. Kawasaki, N. Priel, and G. Gratta, *Phys. Rev. Appl.* **12**, 024037 (2019).
- [39] F. Monteiro, S. Ghosh, A. G. Fine, and D. C. Moore, *Phys. Rev. A* **96**, 063841 (2017).
- [40] National Nuclear Data Center, information extracted from the NuDat3.0 database, <https://www.nndc.bnl.gov/nudat/>.
- [41] M. Frimmer, K. Luszcz, S. Ferreira, V. Jain, E. Hebestreit, and L. Novotny, *Phys. Rev. A* **95**, 061801(R) (2017).
- [42] D. C. Moore, A. D. Rider, and G. Gratta, *Phys. Rev. Lett.* **113**, 251801 (2014).
- [43] F. Monteiro, S. Ghosh, E. C. van Assendelft, and D. C. Moore, *Phys. Rev. A* **97**, 051802(R) (2018).
- [44] E. Gatti and P. F. Manfredi, *Riv. Nuovo Cimento* **9N1**, 1 (1986).
- [45] G. Benato, A. Drobizhev, S. Rajendran, and H. Ramani, *Phys. Rev. D* **99**, 035025 (2019).
- [46] J. B. Dent, B. Dutta, A. Jastram, D. Kim, A. Kubik, R. Mahapatra, S. Rajendran, H. Ramani, A. Thompson, and S. Verma, *Phys. Rev. D* **105**, 015030 (2022).
- [47] M. J. Kristo, in *Handbook of Radioactivity Analysis: Volume 2 (Fourth Edition)*, 4th ed., edited by M. F. L'Annunziata (Academic Press, New York, 2020), pp. 921–951.
- [48] A. Majkowska-Pilip, W. Gaweda, K. Zelechowska-Matysiak, K. Wawrowicz, and A. Bilewicz, *Nanomater. Nanotechnol.* **10**, 1366 (2020).
- [49] U. Holzwarth, I. Ojea Jimenez, and L. Calzolari, *EJNMMI Radiopharmacy Chem.* **3**, 9 (2018).
- [50] N. Wandkowsky, G. Drexlin, F. M. Fränkle, F. Glück, S. Groh, and S. Mertens, *New J. Phys.* **15**, 083040 (2013).
- [51] J. Aalbers *et al.* (LZ Collaboration), *Phys. Rev. D* **108**, 012010 (2023).
- [52] Y. Meng, J. Busenitz, A. Piepke, R. Tsang, M. Wu, and Y. Yao, *J. Instrum.* **17**, P10035 (2022).
- [53] D. Carney, H. Häffner, D. C. Moore, and J. M. Taylor, *Phys. Rev. Lett.* **127**, 061804 (2021).
- [54] M. McEwen *et al.*, *Nat. Phys.* **18**, 107 (2022).
- [55] C. Gonzalez-Ballester, J. Zielińska, M. Rossi, A. Militaru, M. Frimmer, L. Novotny, P. Maurer, and O. Romero-Isart, *PRX Quantum* **4**, 030331 (2023).
- [56] D. Ganapathy *et al.* (LIGO O4 Detector Collaboration), *Phys. Rev. X* **13**, 041021 (2023).
- [57] A. A. Clerk, *Phys. Rev. B* **70**, 245306 (2004).